RSC Pharmaceutics

ROYAL SOCIETY OF CHEMISTRY

PAPER

View Article Online
View Journal | View Issue

Cite this: *RSC Pharm.*, 2025, **2**, 718

Exploiting nano-in-micro-technologies to couple PLGA-hydroxyl-FK866 nanoparticles to a hydrogel network for local drug release†

Eugenia Spessot, ‡[a] Xue Bai,‡§[b] Daniel Moranduzzo,[a] Chen Zhao,[b] Sam Butterworth,[b] Devid Maniglio[a] and Annalisa Tirella *[a,b]

Technological advancements in the formulation and delivery strategies of potent chemotherapeutic agents have been exploited to direct a site-specific drug delivery for the local treatment of tumours. Of these, new generations of nanoparticles are engineered to control the release of therapeutic agents, but they still possess off-target and overall systemic delivery. Injectable hydrogels have unique physico-chemical properties enabling their use as carriers to ensure site-specific targeting. Based on such observations, nanoparticle-loaded hydrogels represent an optimal candidate to both make use of controlled release chemotherapeutic agents (nanoparticles) and local delivery agents (hydrogels) using minimally invasive procedures to reach the target site. Here, we explore the interaction of drug-polymer conjugated nanoparticles with an alginate-based hydrogel network to confine and release a highly cytotoxic compound (hydroxyl-FK866). Specifically, chitosan coating was used to covalently link poly(lactic-*co*-glycolic acid) nanoparticles to oxidised alginate: confinement and interaction of nanoparticles within alginate-based hydrogels were evaluated using atomic force microscopy measurements, confirming the nanoparticle/hydrogel interaction. Deployment of composite injectable hydrogels in 3D printing was finally investigated. Rheological characterisation and printability tests were performed to assess the printability of alginate-based drug delivery systems to match site-specific geometrical requirements. Then, alginate hydrogels loaded with nanoparticles were ionically crosslinked to match the properties of soft tissues (*e.g.* breast tissue). The efficacy of 3D printed hydrogels loaded with a known dose of hydroxyl-FK866 was tested using human breast cancer MDA-MB-231 cells. Results confirmed the expected cytotoxicity, showing approx. 52% toxicity of the hydrogel loaded, after 48 hours of incubation, whereas lower viability (approx. 36%) was measured in cells treated with free nanoparticles (control).

Received 17th December 2024,
Accepted 28th March 2025

DOI: 10.1039/d4pm00334a

rsc.li/RSCPharma

1. Introduction

Systemic administration of anticancer drugs is the most used therapeutic plan, but new strategies are required to tackle significant problems related to poor intra-tumoral drug delivery and off-target effects, as shown in the use of injected nanoparticles.[1] Technological advancements in the formulation and delivery strategies of potent drugs have been exploited to design new therapeutic approaches for the local treatment of tumours, when the surgical procedure and tumour type and size permit it. Local treatment after surgery shows potential to reduce the risk of cancer recurrence and achieve long-term remission.[2] Local drug delivery platforms, for example, peritumoral injections/implants, provide an alternative and reliable approach for cancer therapy, allowing drugs to be delivered directly to the target site at a known dose, bypassing physiological barriers and related issues.[3] In this, it is essential to precisely dose potent drugs and control their release in the surrounding environment.[4,5]

Injectable and transplantable hydrogels have recently received much attention thanks to their biocompatibility, low toxicity, biodegradability and easy synthesis processes, showing great promise as carriers for local drug administration.[6,7] However, when small drugs are loaded in hydrogels, rapid diffusion is observed due to the poor interaction with the hydrogel network, hence limiting their use for

[a]*BIOtech-Center for Biomedical Technologies, Department of Industrial Engineering, University of Trento, Via delle Regole 101, 38123 Trento, Italy.*
E-mail: annalisa.tirella@unitn.it
[b]*Division of Pharmacy and Optometry, School of Health Science, Faculty of Biology, Medicine and Health, University of Manchester, Oxford Road, Manchester M13 9PT, UK. E-mail: annalisa.tirella@manchester.ac.uk*

†Electronic supplementary information (ESI) available. See DOI: https://doi.org/10.1039/d4pm00334a

‡First co-authors.

§Present address: Institute of Food Science and Technology, Chinese Academy of Agricultural Sciences/Key Laboratory of Agro-Products Processing, Ministry of Agriculture, Beijing 100193, China.

local delivery.[8] Drug-loaded nanoparticles (NPs) offer the opportunity not only to load a known dose of therapeutic agent, but also most importantly, they can be engineered to control its release.[9] Exploiting the use of composite hydrogels encapsulating known concentrations of drug-loaded NPs is ground-breaking, offering the unique characteristics of loading compounds at a known dose, confining NPs within hydrogels at known concentrations, matching the mechanical properties of the target tissue, enhancing adhesion to the tissue and most importantly, enabling the localized and sustained release with known kinetics.[10]

In this study, we confined different types of poly(lactic-*co*-glycolic acid) (PLGA) NPs in an alginate-based hydrogel network based on the following two hypotheses: first, positively charged NPs should form 'weak' interactions with the negatively charged alginate chains; secondly, the coating of NPs with primary amines could form covalent and stable bonds with the hydrogel network. Based on our recent work (Bai *et al.*),[11] we used PLGA-based NPs for the sustained release of the highly toxic therapeutic agent hydroxyl-FK866. Chitosan (CS), a linear polysaccharide composed of β(1-4) linked D-glucosamine and *N*-acetyl-D-glucosamine units,[12] was selected to coat PLGA NPs and obtain a homogeneous positively charged surface, also exposing primary amines.

Alginate was selected as it is a non-toxic and biocompatible linear polysaccharide, derived from brown algae, composed of irregular blocks of β-D-mannuronic acid and 1–4 linked α-L-guluronic residues able to form stable ionically cross-linked hydrogels using divalent cations that cannot degrade *in vivo*.[13] Modifications of alginate are used to promote hydrolysis, hence controlling degradation of alginate hydrogels under physiological conditions.[14] Oxidation of alginate is one of the most used approaches to induce degradation of alginate-derived hydrogels, both *in vitro* and *in vivo*.[15] We reported the preparation of oxidized alginates (OAs) with known degrees of oxidation (DOs) and exhibiting an inverse correlation between the degree of oxidation and the molecular weight.[16] We also showed that combinations of alginate, oxidized alginates with varying DOs, and crosslinking strategies can be selected to form hydrogels with known mechanical properties and degradation profiles.[17] Moreover, as OAs presents aldehyde groups proportional to DOs, excess or unreacted groups are still available to react with primary amines (Schiff's base reaction) and form covalent links.[18]

In this study, we used an unmodified alginate and OA at a low degree of oxidation (DO = 5%) loaded with PLGA NPs as injectable technology for the local and sustained release of a potent chemotherapeutic agent: hydroxyl-FK866. Optimization of the chitosan coating of PLGA NPs was performed to direct confinement of PLGA NPs (uncoated, negatively charged) or CS/PLGA NPs (chitosan-coated, positively charged) within the alginate-based hydrogel network. The feasibility of using such formulations as biomaterial inks for the 3D printing of drug delivery technologies was then assessed, and the printability of biomaterial inks was tested at different NP concentrations and without/with chitosan-coating. Interactions between alginate, OA, PLGA NPs and CS/PLGA NPs were investigated using atomic force microscopy (AFM) imaging. AFM allowed us to assess whether positively charged NPs exposing primary amines on their surface could be linked within the negatively charged alginate-based hydrogel network, distinguishing between electrostatic interactions and covalent crosslinks (Schiff's base reaction).[19,20] We found that CS-coated NPs can be effectively linked to the hydrogel network, with high control over their homogeneous distribution across the 3D-printed scaffolds.

Finally, toxicity studies using the human triple-negative breast cancer cell line sensitive to hydroxyl-FK866 (MDA-MB 231) confirmed the expected release of hydroxyl-FK866 with toxicity comparable to NPs dispersed in cell culture media, slightly lower due to diffusion through the hydrogel, as per NPs suspended in cell culture media. We herein show new strategies to load and constrain NPs in degradable hydrogels for local and sustained release of chemotherapeutic agents, further opening the possibility of deploying this formulation for 3D printing of implantable devices with a known geometry, mechanical properties, and *in situ* drug release profiles.

This study demonstrates the broad ramifications of the use of nanoparticles and hydrogels for personalized medicine and shows new strategies to better control the local release of chemotherapeutic agents at the target site. Injectable and 3D printed drug delivery technologies are promising alternatives to increase drug efficacy and reduce inflammatory processes *in situ*, using minimally invasive delivery procedures to limit discomfort to patients.

2. Materials and methods

2.1. Materials

Poly(lactic-*co*-glycolic acid) (PLGA, RG752H, product no. 719919, lactide : glycolide 75 : 25, M_w 4000–15 000), poly(vinyl alcohol) (PVA, product no. 360627-25G), citric acid (product no. 251275), Dulbecco's modified Eagle's medium (DMEM, product no. D6429), fetal bovine serum (FBS, product no. F9665), trypsin (product no. T3924), L-glutamine (product no. G7513), antibiotics (penicillin–streptomycin, product no. P0781), trypan blue (product no. 15250061), cell proliferation reagent WST-1 (product no. CELLPRO-RO), chitosan (CS, product no. 448869-50G), and sodium alginate (ALG, product no. 71238-250G) were all purchased from Sigma-Aldrich (UK). Acetonitrile (HPLC-grade, 34851-2.5L) and methanol (HPLC-grade, product no. 34966-2.5L) were purchased from Honeywell. Hydroxyl-FK866-PLGA was prepared and characterized as described in our previous work.[11] Oxidized alginate with a target degree of oxidation of 5% (OA_5) was prepared and characterized using protocols developed by our group and as described by Zhao *et al.*[16]

2.2. Preparation of FK866-loaded nanoparticles using a microfluidic system

PLGA-based NPs used in this work were prepared using an automated Dolomite microfluidic system (Dolomite, Royston UK) equipped with a 5-input Chip (part no. 3200735), a com-

pressor (part no. 3200117), a Mitos P-Pump (part no. 3200016), Mitos P-Pump Remote Chamber 30 (part no. 3200178), a Mitos Flow Rate Sensor 1–50 μL min^{-1} (part no. 3200098), a Mito Flow Rate Sensor 30–1000 μL min^{-1} (part no. 3200097), a Meros Temperature Control Unite (part no. 3200428), an In-line Valve (part no. 3200087), and a T-Connector (part no. 3000397). Pure HPLC-grade H_2O and a 1% (w/v) PVA solution (aq.) were used as the aqueous (or continuous) phase in all the experiments. The organic (or dispersed) phases were prepared by dissolving PLGA (and derivatives) in acetonitrile at 5.0 mg mL^{-1}. In specific, rhodamine labelled PLGA NPs were used for imaging (Rho-PLGA NPs, ESI SI.1†) and hydroxyl-FK866 loaded NPs for drug delivery studies (hydroxyl-FK866-PLGA NPs, ESI SI.2†). NPs were all prepared using the microfluidic configuration and settings previously optimized: a flow rate ratio of 2 : 3 and a total flow rate of 200 μL min^{-1} at a temperature of 25 °C and a back pressure of 2 bars.[11] Prior to each experiment, aqueous and organic solutions were filtered twice through 0.22 μm PVDF filters (Millex-CV, Merck Millipore Ltd) and 0.2 μm PTFE filters (code 1514-1499, Fisherbrand), respectively. Of note, hydroxyl-FK866-PLGA NPs were used immediately after purification; PLGA and Rho-PLGA NPs were discarded after 2 weeks of storage at 4 °C. All NPs from now on are referred to as PLGA NPs for simplicity unless necessary to specify the formulation.

2.3. Coating of nanoparticles with chitosan

Prior to chitosan (CS) coating, PLGA NPs were concentrated to 40 mg mL^{-1} with dialysis against a 10% w/v PEG 20 kDa (81298, Sigma-Aldrich) solution (aq.) overnight at RT using a dialysis tube (Flot-A-Lyzer G2 dialysis tubes, 3.5–5 kDa membrane cut-off, G235029, Spectra/Por®). CS solutions at a concentration of 0.1% w/v and 0.01% w/v in 4.6 mM HCl (aq.) were mixed with concentrated PLGA NPs in a 1 : 1 dilution and incubated overnight while stirring (RT, 70 rpm) allowing coating. As a control, PLGA NPs were diluted in 4.6 mM HCl solution (aq.) at the same ratio and incubated overnight at RT. Of note, plain PLGA NPs and hydroxyl-FK866-PLGA NPs coated with CS were diluted to final concentrations of 1 mg mL^{-1} and 20 mg mL^{-1} and used to formulate biomaterial inks (Table 1) and hydrogels for imaging (Table 2).

2.4. Physico-chemical characterisation of FK866-nanoparticles

2.4.1. Dynamic light scattering (DLS): *Z*-average size and ζ-potential. PLGA NPs' hydrodynamic diameter (*Z*-average

Table 1 Alginate-based biomaterial inks (hydrogel precursor) for rheological studies, printability and cell culture experiments. PLGA-based nanoparticles without/with chitosan coating and without/with hydroxyl-FK866-PLGA were loaded in the hydrogel precursor at different concentrations (*i.e.*, 1 mg mL^{-1} and 20 mg mL^{-1}), and the highest concentration of NPs was calculated to ensure appropriate release of hydroxyl-FK866 in cell culture experiments

Biomaterial ink ID	ALG (10% w/v)	OA_5 (10% w/v)	HBS	PLGA NPs (1 mg mL^{-1})	PLGA NPs (20 mg mL^{-1})	CS/PLGA NPs (1 mg mL^{-1})	CS/PLGA NPs (20 mg mL^{-1})	Hydroxyl-FK866-PLGA (20 mg mL^{-1})	CS/hydroxyl-FK866-PLGA NPs (20 mg mL^{-1})
1	800 μL	100 μL	100 μL	—	—		—	—	
2	800 μL	100 μL	—	100 μL	—	—	—	—	—
3	800 μL	100 μL	—	—	100 μL	—	—	—	—
4	800 μL	100 μL	—	—	—	100 μL	—	—	—
5	800 μL	100 μL	—	—	—	—	100 μL	—	—
6	800 μL	100 μL	—	—	—	—	—	100 μL	—
7	800 μL	100 μL	—	—	—	—	—	—	100 μL

Abbreviations: ALG: unmodified alginate; OA_5: oxidized alginate, 5% degree of oxidation; HBS: HEPES buffer solution and CS: chitosan.

Table 2 Alginate-based samples used to assess the interaction between NPs and the alginate hydrogel network by atomic force microscopy (AFM) and laser scanning confocal microscopy (LSCM). For sample preparation, alginate-based solutions (aq.) and NP suspensions (aq.) were mixed in a specified volume ratio for a few minutes, and then in the case of AFM the sample solution was pipetted over the sample holder and left to air dry at room temperature for 24 h in a fume hood; whereas for LSCM composite solutions were printed and crosslinked with 50 mM $CaCl_2$ solution (10 min, RT), washed with HBS and imaged immediately after immersion in HBS

Sample_ID	ALG (10% w/v)	OA_5 (10% w/v)	HBS	PLGA NPs (20 mg mL^{-1})	CS/PLGA NPs (20 mg mL^{-1})	PLGA NPs (20 mg mL^{-1})	Rho-PLGA NPs (1 mg mL^{-1})	Rho-PLGA NPs (20 mg mL^{-1})
ALG	5 μL	—	5 μL	—	—	—	—	—
OA_5	—	5 μL	5 μL	—	—	—	—	—
ALG – NPs	5 μL	—	—	5 μL				
OA_5 – NPs		5 μL		5 μL				
ALG – CS/NPs	5 μL		—	—	5 μL			
OA_5 – CS/NPs	—	5 μL	—	—	5 μL			
ALG-OA_5-NPs	800 μL	100 μL				100 μL		
ALG-OA_5-RhoL	800 μL	100 μL	—	—	—		100 μL	
ALG-OA_5-RhoH	800 μL	100 μL	—	—	—			100 μL

size), polydispersity index (PDI), and ζ-potential were measured at 25 °C (pre-equilibration for 2 min) using a Zetasizer Nano ZS (model ZEN3600, Malvern Instruments Ltd, UK) equipped with a solid state HeNe laser (λ = 633 nm) at a scattering angle of 173°. The measurements were performed using a minimum of n = 3 samples (technical replicate) for each group and testing N = 3 independent and separate preparations. Size distributions (Z-average values, PDI) were calculated by applying the general-purpose algorithm and presented as average ± st. deviation of three independent samples.

2.4.2. Transmission electron microscopy (TEM): size and shape. A volume of 3 μL of PLGA NPs was fixed on glow-discharged (25 mA, 1 min) carbon film mesh copper grids using 50 μL of aqueous solution containing 2% (v/v) uranyl acetate stain (negative staining) for 5 min. Grids were left to air dry at RT prior to analysis. Images (N = 3 of each preparation) were acquired using a transmission electron microscope (FEI Tecnai 12 BioTwin) operated at an accelerating voltage of 100 kV.

2.4.3. Determination of the nanoparticle concentration

Dynamic light scattering. Measurements of PLGA NP concentration were performed using Zetasizer software v8.02. Samples scoring a "good particle size distribution sample" (determined automatically by the Zetasizer software when a good quality signal is detected) were used, recording the size and intensity of the sample. To calculate the concentration of NPs, the "concentration utilities calculator" under "tools" – "calculator" of the software was used and the settings were as follows: the final volume was set to 10, the instrument was set to Zetasizer S, and the attenuator was set to 11 (following manufacturers' procedures). Then, the measured sample radius and the refractive index of the material were added to the software, and the nanoparticle concentration was calculated.[21]

Tracking analysis. PLGA NPs' tracking analysis was performed using a NanoSight NS300 instrument and NanoSight NTA 3.4 software, build 3.4.003 (Malvern Panalytical, Malvern, UK). Prior measurements, PLGA NPs were diluted 1 : 500 with deionized water. The diluted samples were then introduced to the NanoSight NS300 instrument. The settings of the camera (sCMOS, laser type: green) were modified to the level of 16. Post-acquisition settings were kept constant between samples and any video files that experienced uncorrected vibration and/or poor tracking analysis were excluded from the final analysis report.

2.5. Nanoparticle-loaded biomaterial ink formulation and characterization

2.5.1. Preparation of biomaterial inks. Biomaterial inks were prepared as reported in Table 1. Briefly, stock solutions of PLGA NPs were prepared at concentrations of 1 mg mL^{-1} and 20 mg mL^{-1}, while unmodified alginate (ALG) and oxidized alginate with a degree of oxidation of 5% (OA_5) were prepared at a concentration of 10% (w/v) by dissolving the powders in distilled water at 37 °C overnight while stirring. Before the experiments, alginate solutions (aq.) and PLGA NP suspensions (aq.) were gently mixed, ensuring homogeneous suspension without air bubble formation.

2.5.2. Rheological properties of alginate-based biomaterial inks. Rheological tests were performed using a Discovery HR-2 hybrid rheometer (TA Instruments, New Castle, Delaware), equipped with a Peltier plate for temperature control. Samples were tested using a stainless-steel cone/plate geometry (50 mm diameter, 2° cone angle, 100 μm truncation gap). To investigate the flow behaviour of biomaterial inks, the solutions were equilibrated at 25 °C and then exposed to a rotational shear rate sweep from 0.1 to 100 s^{-1} to obtain the viscosity curves. The viscoelastic behaviour was assessed with an amplitude sweep test (shear stress ramp from 0.1 to 1000 Pa, 25 °C, 1 Hz). This test was performed to determine the linear viscoelastic region (LVER) and the storage (G') and loss (G'') moduli of the solutions before printing and crosslinking to fix the shape. All tests were performed on n = 3 replicates for each experimental condition reported.

2.5.2. Rheological properties of crosslinked hydrogels. The viscoelastic properties of the hydrogels obtained from the suspensions described in Table 1 were tested on 40 mm diameter and 2 mm thickness cylinders. The Discovery HR-2 hybrid rheometer equipped with a parallel plate geometry (40 mm diameter) was used to perform the tests. Samples were subjected to an oscillation amplitude sweep (0.1–1000.0 Pa, 1.0 Hz) to obtain the extent of the LVER, G' and G'', hence determining the mechanical properties of the alginate-based biomaterial inks. Of note, hydrogel cylinders were obtained by crosslinking the alginate-based suspensions with 50 mM $CaCl_2$ solutions (aq.) and incubating samples for 10 min at RT.

2.6. Assessment of printability

2.6.1. Printing process. Printability studies on PLGA NP loaded alginate-based formulations (Table 1, biomaterial inks **1–5**) were performed using the pneumatic extrusion-based bioprinter, BioX (CELLINK, Boston, USA), equipped with standard printheads. The solution was loaded into a 3 mL disposable cartridge (CELLINK) fitted with a polypropylene standard 25G conical nozzle. Printing was performed on a polystyrene Petri dish at RT and with different combinations of extrusion pressure and printing velocity, as specified for each experiment. Prior to printing, qualitative evaluation of filament formation was performed to identify the minimum extrusion pressure (*data not reported*).

Printability assessment was performed by printing bidimensional geometries (n = 3) at variable pressures (130, 140, and 150 kPa) and printing velocities (5, 10, and 15 mm s^{-1}). Straight lines and grids were printed to quantitatively determine the shape fidelity of the constructs and thus determine the optimal printing parameters.

2.6.2. Image acquisition and processing. For all the printed structures, optical images were acquired with a Dino-Lite AM7915MZTL digital microscope (Dino-Lite Europe, The Netherlands), and then an Otsu threshold was applied using ImageJ software 2017 (NIH, Stapleton, NY, USA). Binary images were then analysed with Matlab 2023a, as described in a previous work.[22]

2.6.3. Printability assessment. Firstly, the uniformity of extruded filaments was quantitatively evaluated on printed

straight lines by calculating the Uniformity ratio (UF), defined in eqn (1) and where p_{ext} is the perimeter of the filament in the post-processed images, L_{th} is the theoretical straight strand length, and t_{av} is the average width of the filament.

The second parameter investigated was the spreading ratio (SR), calculated on the same images acquired for UF by using eqn (2), where t_{av} is the average width of the filament and d_{nozzle} is the internal nozzle diameter (*i.e.*, for the 25 G nozzle d_{nozzle} = 0.250 mm). SR is helpful in determining whether an ink is suitable to print structures with a certain degree of precision and with limited collapse.

The last parameter selected for printability assessment was the printability index (Pr), used to predict the shape retention of an ink and calculated using eqn (3) in which C is the circularity of an enclosed area. Pr is evaluated using a printed geometry 20 × 20 mm squared in the CAD model and with 15% infill density considering the 16 central squares of the grids.[22] If perfectly squared holes are printed, then Pr is equal to 1, while Pr < 1 is found when more circular "collapsed" pores are detected and Pr > 1 indicates irregular shapes and uneven extrusion.

Biomaterial ink **1** was used for preliminary tests to identify optimal printing parameters, and then biomaterial inks **2–4** were assessed, using the printability index Pr to confirm the quality of printed objects.

$$\mathrm{UF} = \frac{\text{extruded perimeter}}{\text{theoretical perimeter}} = \frac{p_{ext}}{L_{th} \times t_{av} \times 2} = \frac{p_{ext}}{p_{th}} \quad (1)$$

$$\mathrm{SR} = \frac{\text{width of extruded strand}}{\text{printing nozzle diameter}} = \frac{t_{av}}{d_{nozzle}} \quad (2)$$

$$\mathrm{Pr} = \frac{\pi}{4} \times \frac{1}{C} = \frac{L^2}{16A} \quad (3)$$

2.7. Laser scanning confocal microscopy (LSCM)

An A1 Laser Microscope (Nikon Instruments Europe BV) was used to acquire volumetric datasets of alginate-based hydrogels with/without rhodamine-labelled PLGA NPs (*i.e.*, Rho-PLGA NPs). PLGA was conjugated with rhodamine following what was described in the literature;[23] then Rho-PLGA NPs were fabricated with microfluidics and characterized in size (ESI, SI.1†). Sections and high-resolution (3D-HR) volumetric datasets were acquired to precisely determine Rho-PLGA NPs' localisation within printed alginate-based hydrogels. For 3D-HR acquisitions, the confocal settings were set as follows: 1 Airy unit, a scan speed of 0.25 frame per s, average line ×2, and 20 μm z-step. Datasets were collected with a Plan Apo 20× DIC M N2 objective and with a 561/595 nm laser. Sections were then processed and analysed using NIS-Element AR 5.30.05, and 3D rendering was performed using NIS-Element AR 5.30.05. Before acquisitions, the bottom and the top levels were determined using the Rho-PLGA NP signal. To compare the amount of particles dispersed in the hydrogels between conditions, images were imported in ImageJ (version 1.51, NIH) and binarised using the Otsu threshold (range 30–240) and the percentage of area occupied by Rho-PLGA NPs was determined with the "analyze particles" tool.

2.8. Atomic force microscopy (AFM)

Surface topography was studied using an NT-MDT Solver Pro system equipped with an S7 scanner. Samples (reported in Table 2) were imaged in semi-contact mode using silicon tips (NSG-11, NT-MDT, 10 nm nominal tip radius, with a resonance frequency of 181 kHz). 500 × 500 nm topography and phase-contrast maps (512 × 512 pixels) were collected on different regions of each sample. Alginate-based solutions (aq.) and NP suspensions (aq.) were mixed in a specified volume ratio for a few minutes, then pipetted over the AFM sample holder and left to air dry at room temperature for 24 h in a fume hood and scanned thereafter. AFM data were analysed with the support of Gwyddion analysis software (v. 2.64).[24]

2.9. Cell experiments

2.9.1. General cell culture. The human breast adenocarcinoma cell line MDA-MB 231 (HTB-26, ATCC) was cultured in DMEM supplemented with 10% (v/v) FBS and 2 mM L-glutamine. MDA-MB-231 cells were routinely cultured and maintained at densities lower than 5×10^4 cells per cm^2 and discarded upon reaching passage number 25. Unless otherwise specified, all cell culture experiments were performed in a humidified 5% (v/v) CO_2 air atmosphere at 37 °C in a complete medium.

2.9.2. Cell proliferation assay. Cell proliferation was determined by measuring the cellular mitochondrial metabolic activity using the WST-1 (water soluble tetrazolium) assay. MDA-MB-231 cells were seeded in 96-well plates (3799, Corning Inc., NY, USA) at a density of 10 000 cells per cm^2 and left to adhere overnight. Alginate-based hydrogels (Table 1) with a volume of 100 μL were prepared under sterile conditions, washed with HBS and included in each well; all the samples were crosslinked with 50 mM $CaCl_2$ (aq.) for 10 min. Hydroxyl-FK866-PLGA NPs were prepared as described in our previous work and characterized in size and surface charge without and with CS coating (ESI SI.2†). Biomaterial inks **6** and **7** (Table 1) were immersed in the cell culture medium and incubated for 48 h; biomaterial inks **1** and **5** (Table 1) and untreated cells were used as positive controls, whereas cells treated with 30% (v/v) methanol were used as negative controls. Of note, the amount of hydroxyl-FK866-PLGA NPs loaded in alginate hydrogels was calculated based on our recent study and determined as a final 20 mg mL^{-1} concentration of hydroxyl-FK866-PLGA NPs.[11] After incubation for 48 h, the hydrogel and cell culture media were removed from each well, and cells were washed with PBS (n = 3) and then incubated with WST-1 reagent (1 h, 37 °C). Experiments were performed with n = 3 replicates and repeated (N = 2) with biological independent experiments.

2.10. Statistical analysis

All data represent the mean of a minimum of three independent experiments ± standard deviation (st. dev.), unless other-

wise stated. Statistical analyses were performed by one-way ANOVA, followed by Sidak's multiple comparison tests in GraphPad Prism 9. Differences were considered significant at $p < 0.05$ ($*p \leq 0.05$, $**p \leq 0.01$, $***p \leq 0.001$, and $****p \leq 0.0001$).

3. Results and discussion

3.1. Nanoparticle characterisation

As reported in our recent work, acid-terminated PLGA in acetonitrile (organic phase) and PVA solution (aq.) (aqueous phase) were used to prepare PLGA NPs with the Dolomite microfluidic system.[11] PLGA NPs have a mean *Z*-average size of 207 ± 15 nm and negative ζ-potential (−21.90 ± 2.13 mV) due to the presence of carboxylic end groups in PLGA. CS-coated PLGA NPs have larger hydrodynamic size, showing an increase in NP size (218 ± 4 nm and 245 ± 20 nm) with increased concentrations of CS (0.01% w/v *vs.* 0.1% w/v) (Table S1†), as reported in similar studies.[25,26] As expected, non-coated NPs have a lower PDI (0.118 ± 0.007) when compared to CS-coated NPs (0.207 ± 0.024 and 0.256 ± 0.025, respectively for 0.01% w/v CS and 0.1 w/v CS). Of note, all NPs have PDI < 0.3, which indicates a monodispersed particle size in all formulations tested (Table S1†).

PLGA NPs with low concentrations of CS (0.01% w/v) showed an increase in the ζ-potential (23.00 ± 4.32 mV), indicating the successful coating and the presence of positive charge on NPs' surface due to the protonation of amine groups in chitosan. When a higher concentration of CS is used to coat NPs (0.1% w/v), an increase in the ζ-potential (49.33 ± 1.25 mV) was observed and found to be proportional to the CS concentration used. For this reason, and as the ζ-potential impacts on particle stability, cell adhesion and interaction with negatively charged biomaterials,[18] it was decided to further use CS-coated PLGA NPs obtained with higher concentrations of CS (*i.e.*, 0.1% w/v, Fig. S2†).

TEM images confirmed that the coating process did not impact the morphology of PLGA NPs, with all NPs showing a spherical morphology (Fig. 1E and F). Furthermore, TEM images do not demonstrate variations in the size of PLGA NPs without/with CS coating; the slight increase in size measured by DLS could be caused by the presence of a hydrated thin layer of CS (proportional to CS concentration used in the NP coating step) and not detected in dry particles analysed by TEM (Fig. S3†).

NanoSight tracking analysis was further used to determine the concentration of CS/PLGA NPs (obtained with the optimised protocol, 0.1% w/v CS concentration) and the uncoated control in the dispersed phase. The precise quantification of NP concentration is considered essential to further dose hydroxyl-FK866-PLGA NPs in the alginate-based hydrogels for further drug delivery studies.[27] Herein, we compared two methods to determine the concentrations of PLGA nanoparticles: NanoSight and DLS. The concentrations of uncoated PLGA NPs measured in both methods are similar, that is, (2.68 ± 0.61) × 10^7 particles and (2.46 ± 0.34) × 10^7 particles, measured respectively with DLS and NanoSight. In the case of CS/PLGA NPs, variations in the measured concentrations are observed (in the range of 15–20%). Again, differences in the

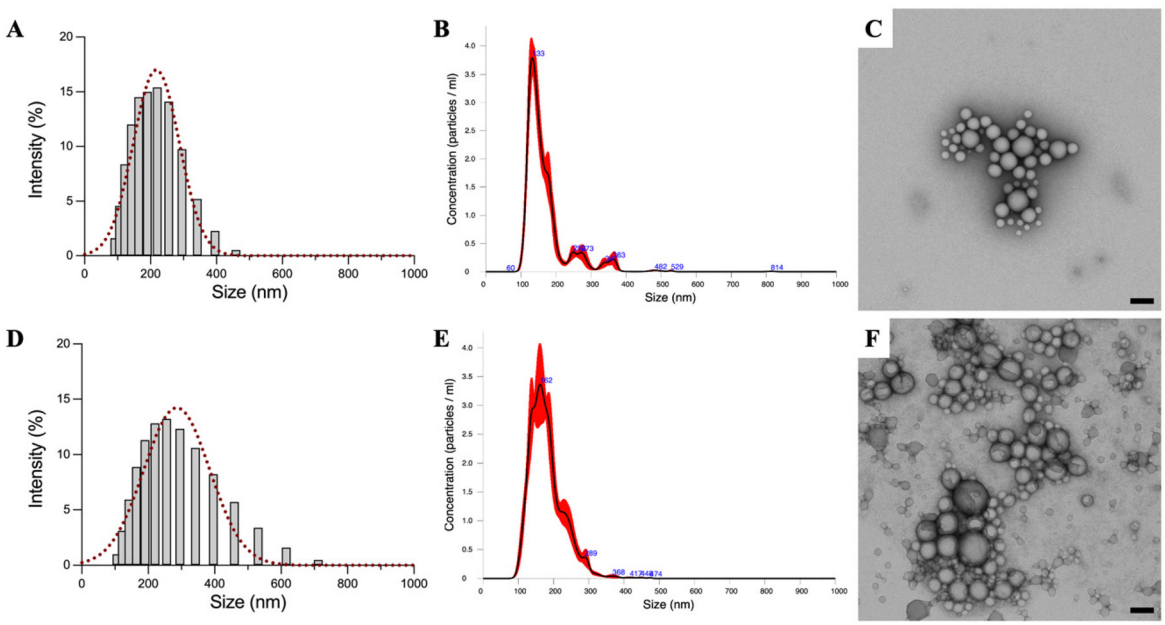

Fig. 1 Characterization of PLGA NPs: (A) DLS size distribution (grey bars) and fitting (red dotted line), (B) NanoSight size analysis, and (C) TEM micrographs. Characterization of CS/PLGA NPs: (D) DLS size distribution (grey bars) and fitting (red dotted line), (E) NanoSight size analysis, and (F) TEM micrographs. NPs were prepared with microfluidics and then coated using 0.1% w/v chitosan in 4.6 mM HCl (aq.) solution. TEM image scale bars: 200 nm.

detection method (light scattering *vs.* image analysis) could affect the returned measure in the presence of the CS layer: a concentration of $(3.98 \pm 0.17) \times 10^8$ CS/PLGA NPs is measured with DLS being much higher than the $(3.30 \pm 0.02) \times 10^7$ CS/PLGA NPs detected by the Nanosight, and more similar to the controls.

3.2. Rheology

The rheological properties were evaluated on the materials before (biomaterial ink) and after printing (crosslinked hydrogel), as previously reported.[28–30] Firstly, the viscosity and viscoelasticity of biomaterial inks (*i.e.*, aqueous polymeric solution) before printing were analysed to assess their flow properties and suitability to be processed with extrusion-based bioprinters. Of note, this characterisation could be used to evaluate their injectability. Then, the viscoelastic properties of the crosslinked hydrogels were analysed to compare the mechanical properties of the hydrogels to those of breast tissues, both healthy and tumoral.

3.2.1. Pre-printing stage: rheological properties of the biomaterial inks. The properties of the biomaterial inks were evaluated before printing since they are (A) directly correlated with the extrudability of the material and (B) related to the printability in extrusion bioprinters. The shear thinning behaviour is an ideal requirement in biomaterial inks as it allows a material to flow and be extruded through the nozzle under high shear stress and to retain its initial viscosity once printed on a surface. As shown in Fig. 2A, the viscosity of biomaterial inks (**1–5**, Table 1) decreases with an increase in the shear rate, showing a marked shear thinning behaviour similar in all the conditions, suggesting their suitability to inks for extrusion bioprinting.

The viscoelastic properties of the biomaterial inks before extrusion have been assessed; an example of the flowing properties of the biomaterial ink **3** (Table 1) is shown in Fig. 2B, highlighting the presence of yield stresses and showing that the biomaterial ink behaves as a viscous fluid ($G'' > G'$). This was as expected since the solutions tested were not crosslinked before extrusion. Moreover, the yield stress, which delimits the linear viscoelastic region, occurred at around 400 Pa, predicting the possibility of printing these solutions.[29] In fact, previous studies reported that values of yield stress higher than 100 Pa led to acceptable printing outcomes.[30–33]

3.2.2. Post-printing stage: mechanical properties of the crosslinked hydrogels. After printing, biomaterial inks were crosslinked (50 mM $CaCl_2$ (aq.), 10 min, RT), and the mechanical properties of the obtained hydrogels were tested in the oscillatory mode (Fig. 2C); the obtained values were used to confirm matching with the ones of human soft tissues. The values of the storage (G') and loss (G'') moduli were similar for all the tested samples with average values of 30–35 kPa and 4–7 kPa, respectively (Fig. 2D). The obtained G' values were comparable with the mechanical properties of pathological breast tissues (*e.g.*, fibrous, advanced cancerous states). In fact, the average elastic modulus of pathological breast tissue was calculated with several techniques on both *in vivo* and *ex vivo* tissues with reported results in the range of 4–94 kPa, usually 3–6 times higher than the mechanical properties of healthy breast tissues.[34] The mechanical properties of the hydrogels herein proposed are consistent with what was reported by Shpaisman *et al.*, in which a poly(ethylene glycol) and desami-

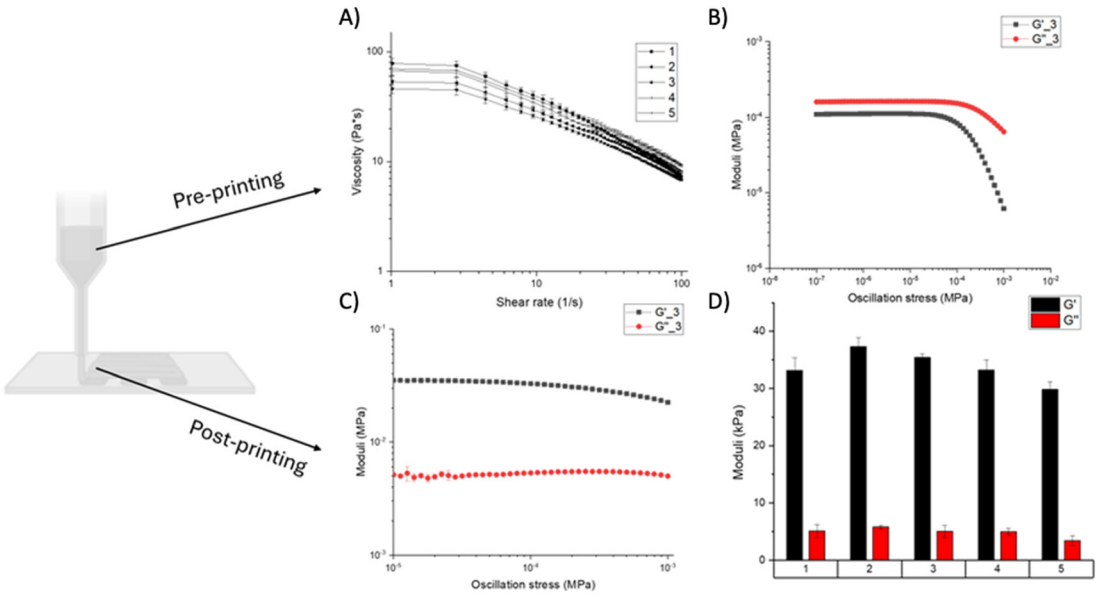

Fig. 2 (A) Viscosity average curves for all the tested conditions acquired with a rotational shear rate sweep. (B) Oscillatory stress sweep tests for biomaterial ink **3** before extrusion, as representative curves for all the conditions. (C) Oscillatory stress sweep tests for biomaterial ink **3** crosslinked, as representative curves for all the conditions. (D) Mean storage and loss moduli acquired from oscillatory stress sweep tests in the linear viscoelastic region of the crosslinked inks. For biomaterial inks composition refer to Table 1. Data presented as average ± st. dev. (n = 3).

notyrosyl-tyrosine ethyl ester hydrogel was designed as a soft tissue filler after tumour removal for curcumin release and having compressive moduli in the range of 7–100 kPa.[35]

Additionally, results showed that the presence of PLGA NPs (without/with CS coating) did not impact the hydrogel mechanical properties due to a low dispersion of particles in the hydrogel network. All hydrogels showed $G' > G''$, denoting the dominant elastic character of hydrogels, which suggested a completely gelled and elastic structure driven only by the presence of physical ionic bonds, and with the presence of viscous components.[36]

3.3. Printability assessment

Three-dimensional (3D) printability of a biomaterial ink is defined as the ability of a hydrogel to form and maintain a reproducible 3D structure with dimensional integrity.[37] Rheological properties and printing parameters, such as extrusion pressure and speed, can affect print quality. For example, a low pressure would lead to biomaterial ink extrusion failure, a high pressure could cause poor printability, and a low printing speed would result in a high quantity of extruded material per unit time, resulting in poor printability. High-speed print nozzles can also result in discontinuous filaments.[38]

In this study, firstly we defined the optimal printing parameters for the biomaterial ink **1** (without NPs) as we did not find differences in the rheological properties of the biomaterial inks with PLGA NPs (Fig. 2A). Then, we validated the optimal printing parameters for the biomaterial ink **3** with the highest concentration of PLGA NPs (20 mg mL^{-1}) and the biomaterial ink **5** with 20 mg mL^{-1} CS/PLGA NPs (Table 1) as shown in Fig. 3F.

The UF and the SR of biomaterial ink **1** at different pressures/velocities were evaluated on a simple printed line (Fig. 3A). UF values close to 1 (Fig. 3B) were found for most of the tested parameters, which is the ideal value as UF = 1 is an indication of a smooth extrusion, while UF > 1 represents over-gelated hydrogels.

This result was as expected since the biomaterial ink **1** has a viscous-like behaviour with $G'' > G'$. From the analysis of the SR, it is possible to observe that all the tested combinations have SR > 1 (Fig. 3C). Thus, they have a higher width than the one designed with the CAD. However, SR values below 2 are rarely present in the literature due to the viscoelastic nature of the material used, due to the relaxation of the polymeric chains. SR is lower with the decrease of pressure and increase in velocity.

To quantitatively evaluate the shape fidelity of biomaterial ink **1**, we evaluated the Pr values and grid morphology under different pressures and speeds (Fig. 3D and E). In specific, biomaterial ink **1** ensured adequate flow conditions, with smooth and uniform filaments being continuously extruded, whilst having perfect printability state of geometries with square-shaped interconnecting channels and Pr values of 1; literature reports that when Pr is in the range of 0.8–1.1, the 3D printed hydrogel structures will exhibit good filament morphology and mechanical stability.[39]

We used biomaterial ink **1** for all printability tests and selected the combination of pressure and velocity which had

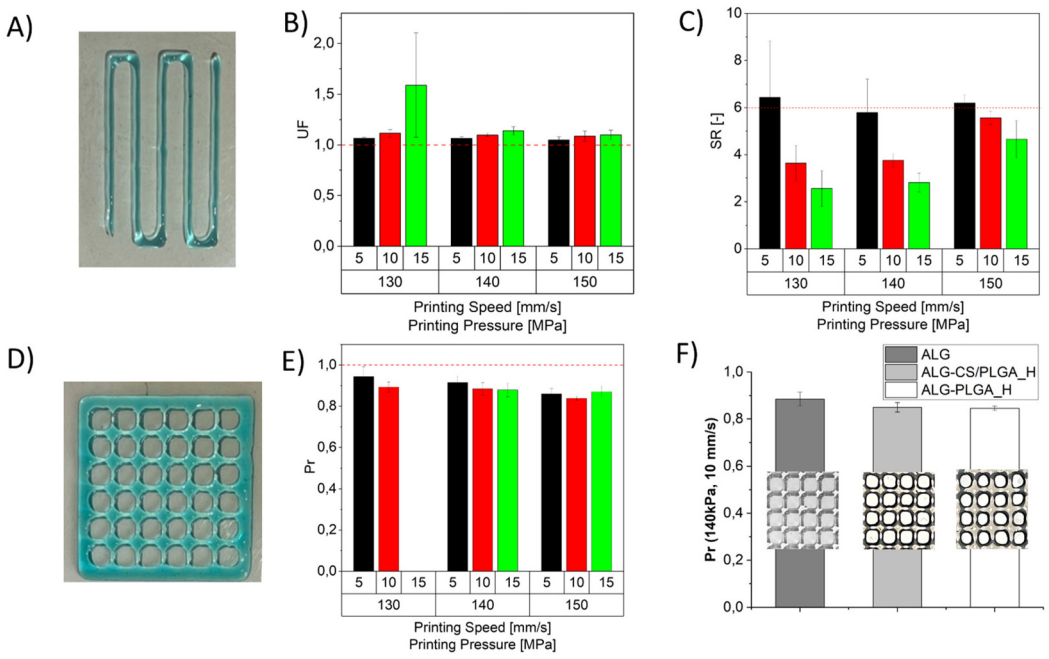

Fig. 3 Assessment of printability on the alginate-based biomaterial ink: (A) example of the printed straight lines used for the quantitative analysis of (B) uniformity ratio and (C) spreading ratio by varying the extrusion pressure and the printing speed and (D) example of the printed grid used for the determination of (E) printability index. Results are expressed as mean ± st. dev. (n = 3) of tests performed using biomaterial ink **1**. (F) Comparison of printability index biomaterial inks **1**, **3** and **5** using the optimal printing parameters of 140 kPa and 10 mm s^{-1}. Micrographs in the figure show a representative layer for each biomaterial ink used.

the lowest SR and a Pr value close to 1 as the optimal printing parameters. Thus, the optimal printing parameters were 140 kPa and 10 mm s^{-1}.

Then, we evaluated the shape fidelity with the measure of the printability index of different biomaterial inks (*i.e.*, biomaterial ink **1**, biomaterial ink **3** and biomaterial ink **5**, Table 1) printed with the optimal parameters; as shown in Fig. 3F, all biomaterial inks used have good printability and the presence of the NPs (regardless of the CS coating) does not affect the printability of the biomaterial ink.

3.4. Composite alginate-based hydrogels: interaction and distribution of PLGA-NPs in the hydrogel

Two distinctive imaging acquisition methods were used: atomic force microscopy (AFM) to interrogate the interaction between PLGA and CS/PLGA NPs and the alginate network and understand if any physical and/or chemical interaction may occur and laser scanning confocal microscopy (LSCM) to assess volumetric distribution of Rho-PLGA NPs within alginate-based hydrogels (Table 2). Of note, and due to the relatively low concentration of PLGA NPs used in the formulation of biomaterial inks, higher concentrations of PLGA NPs and different alginate formulations were selected to better evaluate the interactions occurring between positive (CS/PLGA NPs) and negative (PLGA NPs) charges within the hydrogel network (supposedly negative, due to the presence of hydrated alginate chains), and the concentration of PLGA NPs was increased only for sample preparation for AFM studies (Table 2).

3.4.1. Interaction between nanoparticles and the hydrogel network: AFM. AFM was used to investigate the surface interactions between PLGA NPs and alginates. AFM analyses were conducted on alginate-based dry films as in Table 2 acquiring 500 × 500 nm scan size areas to investigate the particle/matrix interface (Fig. 4). Results represent both topography and phase contrast images, with the latter used to highlight the differences among the samples and assist the interpretation of the sample's topography.

Both alginate films (ALG and OA_5) were characterised by a granular structure, as expected. While in the case of ALG, grains are characterised by an elongated shape ranging several hundred microns, and OA_5 grains are more circular, with a diameter of a few tenths microns (Fig. 4B, phase contrast). This confirms our previous study that the oxidation of alginate causes a reduction of the molecular weight.[16]

The loading of uncoated PLGA NPs (207 ± 20 nm; −21.90 ± 2.73 mV) showed different interactions as a function of the polysaccharide used. An evident segregation of NPs at the surface with ALG with poor interfacial affinity is observed, possibly due to the negative charge of both PLGA NPs and ALG, which is emphasized by the film retraction caused by the

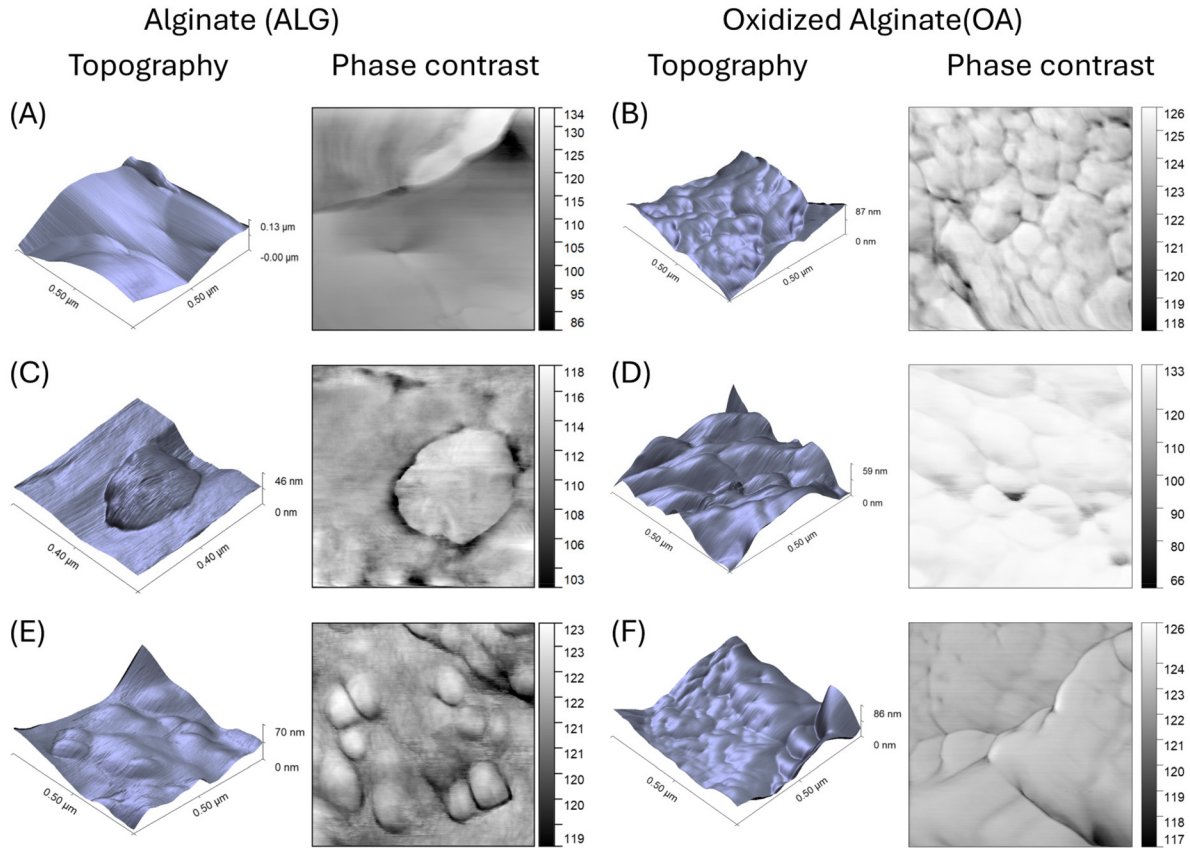

Fig. 4 AFM images of topography and phase contrast images of a 500 × 500 nm scan area of: (A) ALG; (B) OA_5; (C) ALG-PLGA NPs; (D) OA_5-PLGA NPs; (E) ALG-CS/PLGA NPs; and (F) OA_5-CS/PLGA NPs.

polymer drying (Fig. 4C). Differently, when PLGA NPs are embedded in OA_5 (Fig. 4D), a higher interaction is observed between NPs and the modified polysaccharide matrix, with no evidence of surface segregation and no significant difference in morphology from that of a pure OA_5 film (Fig. 4B) with a slight enhancement of the globular edges.

The loading of CS/PLGA NPs (245 ± 20 nm, +49.33 ± 1.25 mV) within alginate-based solutions showed different levels of interactions with the alginates. In the case of ALG (Fig. 4E), there is still some level of segregation between particles and matrix; however, the nanoparticles are visible at the surface and appear to be coated by an alginate layer. This phenomenon is probably due to the opposite charges that characterise ALG (negatively charged) and CS/PLGA NPs (positively charged), which resulted in an overall improvement of the interfacial interactions. Interestingly, OA_5 and CS/PLGA NPs show no evidence of NP segregation at the surfaces (Fig. 4F), suggesting a further degree of interaction between the primary amine group on CS chains (hence on the NP surface) and the aldehyde groups on oxidized alginate. Moreover, and as observed for the OA_5 and PLGA NPs composite hydrogel (Fig. 4D), the globular morphology of the OA_5 matrix is enhanced with respect to ALG, leading to a slight increase in the Z topography profile.

3.4.2. Distribution of nanoparticles in the hydrogel: LSCM. LSCM acquisition was performed on hydrated and crosslinked 3D-printed samples to assess the homogeneous distribution of PLGA NPs. Biomaterial inks loaded with Rho-PLGA NPs (ESI, SI.1,† Fig. S1†) were mixed as described in Table 2, using biomaterial ink **3** (Table 1) as the control, to investigate how the mixing and the printing processes impacted the distribution of PLGA NPs within the alginate-based biomaterial ink. As shown in Fig. 5A, and as expected, no signal was detected for biomaterial ink **3**, whereas two different nanoparticle distributions were observed with a detected signal proportional to the concentration of Rho-PLGA NPs used (Fig. 5B and C) and calculated as the percentage of area occupied by the particles per image (Fig. 5D). As shown in Fig. 5C, 20 mg mL^{-1} Rho-PLGA NPs are homogeneously dispersed across the hydrogel network after printing and crosslinking, proving the possibility to use this formulation to load and confine NPs for local drug delivery.

3.5. Cytotoxicity of hydrogels loaded with hydroxyl-FK866-PLGA NPs

Hydroxyl-FK866, a cytotoxic compound, is a highly specific inhibitor of the biosynthesis of the coenzyme nicotinamide adenine dinucleotide, which could be used for cancer treat-

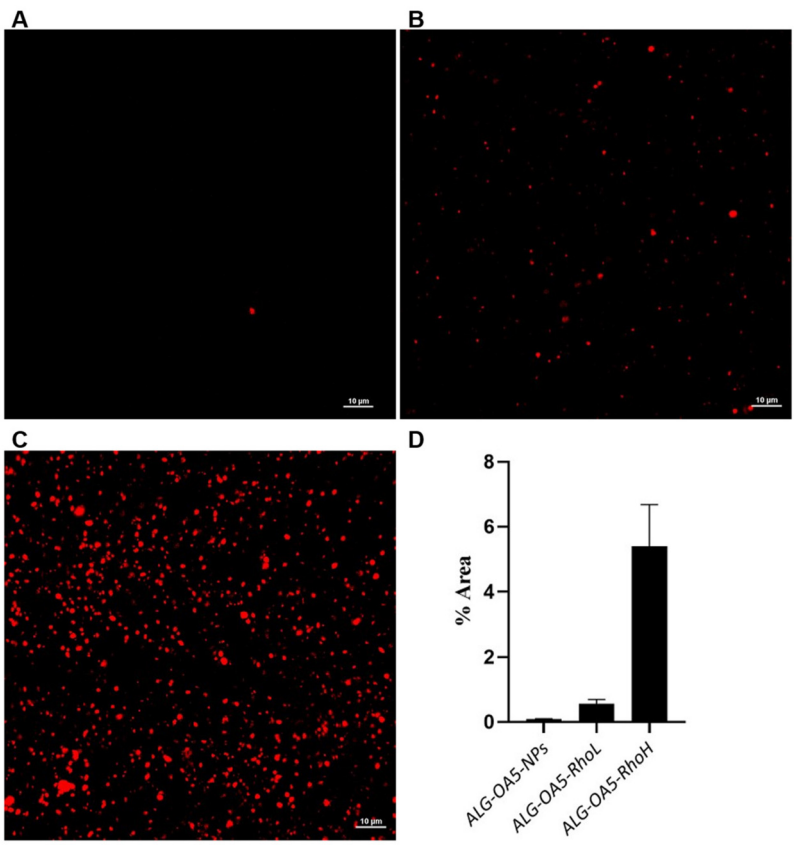

Fig. 5 LSCM images of PLGA NPs in alginate-based biomaterial inks crosslinked with 50 mM $CaCl_2$ solution (aq.): (A) biomaterial ink **3** (*i.e.*, 9% w/v ALG-OA_5 loaded with 20 mg mL^{-1} PLGA NPs); (B) 1 mg mL^{-1} Rho-PLGA NPs and (C) 20 mg mL^{-1} Rho-PLGA NPs loaded in ALG-OA_5 hydrogels. Scale bars: 10 µm. (D) Percentage of area covered by the particles per image. Data are presented as mean ± st. dev. (n = 3).

ment. In our previous work, we have shown that hydroxyl-FK866-PLGA NPs are able to release hydroxyl-FK866 by a hydrolytically cleavable linkage for up to 3 months under physiological conditions with effective toxicity to cancer cells (Fig. S2A†).[11]

The hydroxyl-FK866-PLGA NPs used in this work have an encapsulation efficiency of 98.6 ± 5.8% (*data not shown*). The presence of CS coating slightly increases the *Z*-average size of NPs (Fig. S2B†), as well as switching the ζ-potential from negative (hydroxyl-FK866-PLGA NPs) to positive (CS/hydroxyl-FK866-PLGA NPs) values (Fig. S2C†).

Prior to loading in biomaterial inks, the toxicity of hydroxyl-FK866-PLGA NPs was assessed using PLGA NPs as controls (Fig. 6A). As expected, the drug-loaded NPs were toxic to the cells regardless of the presence of CS coating (no statistical difference between hydroxyl-FK866-PLGA NPs and CS/hydroxyl-FK866-PLGA NPs); in specific, the release of hydroxyl-FK866 impacted cell viability more than the charge of NPs (typically positively charged NPs are reported to be more toxic[40]). Of note, the concentration of CS used to coat NPs is well reported in the literature and found to not impact cell viability;[41,42] our study aligns with the literature, showing no significant difference in viability between CS/PLGA NPs and untreated controls (Fig. 6A).

Then, sterile biomaterial inks **1**, **5**, **6** and **7** were formulated (Table 1), crosslinked with 50 mM sterile $CaCl_2$ solution (aq.) and hydrogels incubated with MDA-MB-231 cells.

All nanoparticles used (*i.e.*, CS/PLGA NPs, hydroxyl-FK866-PLGA NPs and CS/hydroxyl-FK866-PLGA NPs) were at a concentration of 20 mg mL^{-1}, concentration previously selected as ensuring release of hydroxyl-FK866 at toxic doses in the observed time point (48 h). Alginate only hydrogel (biomaterial ink **1**) and CS/PLGA NP loaded alginate hydrogels (biomaterial ink **5**) were well tolerated by cells, showing viability of 90–95% and similar to untreated control (100%, Fig. 6B). As expected, and regardless of the presence of CS coating, both hydrogels loading hydroxyl-FK866-PLGA NPs were found to be toxic (biomaterial inks **6** and **7**), without statistically significant difference at the observed timepoint.

These results showed that the viability of cells treated with drug-loaded NPs dispersed in a medium (hydroxyl-FK866-PLGA NPs and CS/hydroxyl-FK866-PLGA NPs, Fig. 6A) was lower than the one observed when the same NPs were loaded in alginate hydrogels (Fig. 6B), being 36 ± 1% *vs.* 52 ± 2%. Such different cell responses could be explained considering that hydroxyl-FK866 released by NPs in a hydrogel should diffuse throughout the polysaccharide matrix and, thus, is made available to cells with a delay.

In this work, we used a small hydrophilic cytotoxic compound (hydroxyl-FK866) with molecular weight (MW) well below the one of alginate.[16] Considering that the diffusion coefficient of molecules with MW < 2×10^4 in alginate hydrogels is similar to those in the water system,[43] it was possible to assume that no difference was present in the diffusive profiles of hydroxyl-FK866 within alginate hydrogels. Therefore, the only driving force for hydroxyl-FK866 release resides in the hydrolysis from PLGA in hydroxyl-FK866-PLGA NPs, hence depending on the pH of the microenvironment. Since alginate hydrogels can immediately reach an equilibrium with the environment pH,[43,44] it is possible to assume that the

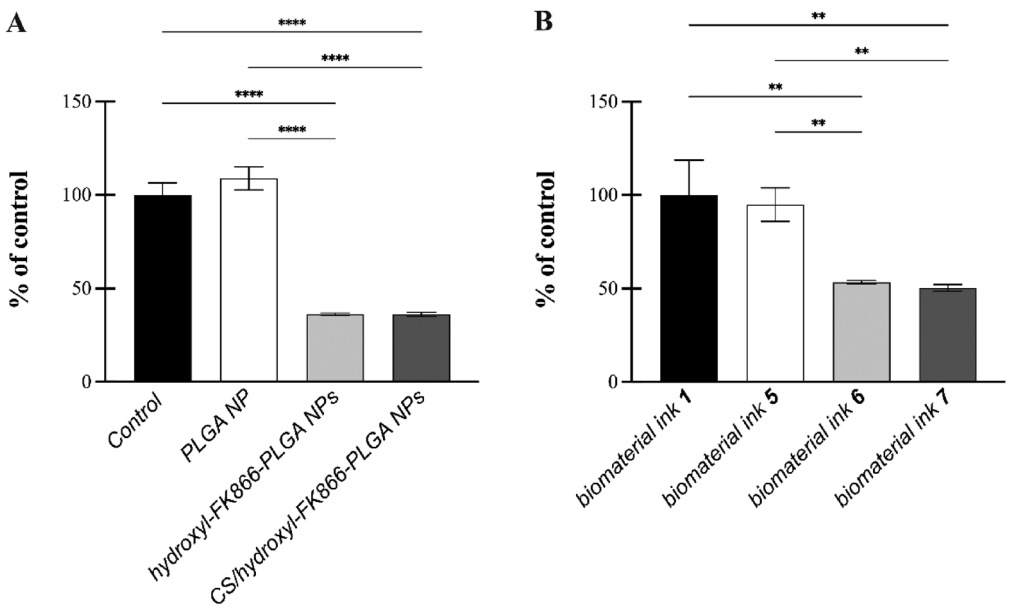

Fig. 6 Cell proliferation was determined using the WST-1 assay representing viability using (A) nanoparticles and (B) printed nanoparticle-loaded hydrogels. NPs = nanoparticles; Gel = alginate hydrogel; HBS = HEPES-buffered saline; CS = chitosan; drug-loaded uncoated NPs = hydroxyl-FK866-PLGA nanoparticles without chitosan coating; drug-loaded CS-coated NPs = hydroxyl-FK866-PLGA nanoparticles coated with chitosan. Data are presented as mean ± st. dev. of $n = 3$ replicates and $N = 2$ biological independent experiments. Differences were considered significant at $p < 0.05$ (*$p \leq 0.05$, **$p \leq 0.01$, ***$p \leq 0.001$, ****$p \leq 0.0001$).

hydroxyl-FK866-PLGA NPs are exposed to a constant pH. In our previous study,[11] the effective release of hydroxyl-FK866 was characterized at different pH values, mimicking both the tumoral (pH = 6.4) and healthy (pH 7.4) environmental pH of breast tissues and with results displaying a prolonged release of low doses of the cytotoxic compound up to two months.

Overall, results show that alginate-based hydrogels could act as depot drug delivery systems for different treatments, such as cancer. Based on our previous work, we can corroborate that hydroxyl-FK866-PLGA NPs could provide sustained release even when loaded and interlinked in the polysaccharide network, constraining NPs at a given location and ensuring the release of the therapeutic for prolonged periods of time, thereby minimizing systemic toxicity and reducing dosing frequency.

4. Conclusions

A novel alginate-based biomaterial ink loading and confining PLGA NPs for the localised and sustained release of potent cytotoxic compounds for cancer treatment has been presented in this study. CS/PLGA NPs were found homogeneously dispersed and confined within oxidized alginate (OA_5) hydrogels *via* covalent crosslinks (primary amines and aldehydes). Composite biomaterial inks (9% w/v ALG-OA_5; 20 mg mL^{-1} PLGA NPs) showed shear thinning properties with excellent printability (mean Pr in the range of 0.80–0.95). Rheological characterization of composite hydrogels showed mechanical properties compatible with soft tissues (*e.g.*, breast tissue) and, overall, in line with the maintenance of cell phenotype and not triggering inflammatory responses due to mechanical mismatch. Combinations of hydroxyl-FK866-PLGA NPs and alginates were used to treat triple-negative human breast cancer (MDA-MB-231), showing toxicity of all drug-loaded systems (30–40% viability at 48 h) when compared to the controls. This study demonstrates the loading and confinement of highly toxic compounds (CS/hydroxyl-FK866-PLGA NPs) within injectable alginate-based hydrogels for the local treatment of solid tumours. Such a hybrid system can facilitate the delivery of toxic small chemotherapeutics at the tumour site, improving the efficacy of treatments against cancer cells. Further long-term *in vitro* studies are required to clearly demonstrate the effectiveness in the local and sustained release of hydroxyl-FK866, as well as the confinement of CS/PLGA NPs in modified alginate hydrogels for both *in vitro* and *in vivo* applications.

Author contributions

Eugenia Spessot and Xue Bai are responsible for conceptualization, data curation, formal analysis, investigation, methodology, validation, visualization, writing – original draft, and writing – review & editing. Daniel Moranduzzo is responsible for methodology, formal analysis and visualization. Chen Zhao is responsible for methodology. Sam Butterworth is responsible for conceptualization, supervision, funding acquisition and writing – review & editing. Devid Maniglio is responsible for formal analysis, methodology, visualization and writing – review & editing. Annalisa Tirella is responsible for conceptualization, data curation, formal analysis, funding acquisition, supervision, visualisation, and writing – review & editing.

Data availability

The data supporting this article have been included as part of the ESI.†

Conflicts of interest

The authors declare that they have no known competing financial interests or personal relationships that could have appeared to influence the work reported in this paper.

Acknowledgements

All the authors would like to thank Prof. Michela Denti and Miss Ilaria Brentari (Department of Cellular, Computational and Integrative Biology, University of Trento, Italy) for their help in the acquisition and interpretation of NanoSight data. XB is grateful to Dr Francesca Agostinacchio (Biotech – Department of Industrial Engineering, University of Trento, Italy) for the help in the acquisition of confocal microscopy images. ES and AT are grateful for the support of Fondazione VRT. ES, DM, and AT acknowledge the SHIFT Project, funded by the European Union's Horizon 2020 Research and Innovation Programme under the Maria Sklodowska-Curie grant agreement no. 101008041.

References

1 C. Pacheco, A. Baião, T. Ding, W. Cui and B. Sarmento, *Adv. Drug Delivery Rev.*, 2023, **194**, 114724.
2 Q. Leng, Y. Li, P. Zhou, K. Xiong, Y. Lu, Y. Cui, B. Wang, Z. Wu, L. Zhao and S. Fu, *Mater. Sci. Eng., C*, 2021, **129**, 112390.
3 A. Spadea, A. Tirella, J. M. Rios de la Rosa, E. Lallana, M. Mehibel, B. Telfer, N. Tirelli, M. J. Lawrence, K. J. Williams, I. J. Stratford and M. Ashford, *Pharmaceutics*, 2024, **16**, 1286.
4 Y. Xie, M. Liu, C. Cai, C. Ye, T. Guo, K. Yang, H. Xiao, X. Tang and H. Liu, *Front. Oncol.*, 2023, DOI: **10.3389/fonc.2023.1027254**.
5 J. Zheng, X. Song, Z. Yang, C. Yin, W. Luo, C. Yin, Y. Ni, Y. Wang and Y. Zhang, *J. Controlled Release*, 2022, **350**, 898–921.
6 X. Bai and A. Tirella, *Int. J. Drug Discovery Pharmacol.*, 2022, 10–10.

7 F. Perin, E. Spessot and A. Motta, in *Multiscale Cell-Biomaterials Interplay in Musculoskeletal Tissue Engineering and Regenerative Medicine*, ed. J. M. Oliveira, R. L. Reis and S. Pina, Academic Press, 2024, pp. 219–240.
8 J. Min Jung, Y. Lip Jung, S. Han Kim, D. Sung Lee and T. Thambi, *J. Colloid Interface Sci.*, 2023, **636**, 328–340.
9 I. V. Zelepukin, O. Y. Griaznova, K. G. Shevchenko, A. V. Ivanov, E. V. Baidyuk, N. B. Serejnikova, A. B. Volovetskiy, S. M. Deyev and A. V. Zvyagin, *Nat. Commun.*, 2022, **13**, 6910.
10 Y. Jiang, N. Krishnan, J. Heo, R. H. Fang and L. Zhang, *J. Controlled Release*, 2020, **324**, 505–521.
11 X. Bai, S. Tang, S. Butterworth and A. Tirella, *Biomater. Adv.*, 2023, **154**, 213649.
12 Y. A. Khan, K. Ozaltin, A. Bernal-Ballen and A. Di Martino, *J. Drug Delivery Sci. Technol.*, 2021, **61**, 102126.
13 F. Abasalizadeh, S. V. Moghaddam, E. Alizadeh, E. Akbari, E. Kashani, S. M. B. Fazljou, M. Torbati and A. Akbarzadeh, *J. Biol. Eng.*, 2020, **14**, 8.
14 C. Gao, M. Liu, J. Chen and X. Zhang, *Polym. Degrad. Stab.*, 2009, **94**, 1405–1410.
15 T. Boontheekul, H.-J. Kong and D. J. Mooney, *Biomaterials*, 2005, **26**, 2455–2465.
16 C. Zhao, A. Latif, K. J. Williams and A. Tirella, *React. Funct. Polym.*, 2022, **175**, 105292.
17 A. Bucciarelli, C. Zhao, X. Bai, A. Latif, K. Williams and A. Tirella, *ChemRxiv*, 2023, preprint, DOI: **10.26434/chemrxiv-2023-7bt78**.
18 I. A. Duceac and S. Coseri, *Gels*, 2022, **8**, 779.
19 N. Amiryaghoubi, M. Fathi, A. Safary, Y. Javadzadeh and Y. Omidi, *Int. J. Biol. Macromol.*, 2024, **256**, 128335.
20 S. E. Samuel, T. Ghosh, A. Damodar Nayak, R. Deveswaran and B. V. Basavaraj, *J. Drug Delivery Sci. Technol.*, 2024, **97**, 105746.
21 Zetasizer family software update v8.02, **https://www.malvernpanalytical.com/en/support/product-support/software/zetasizer-family-software-update-v8-02**, (accessed 25 October 2024).
22 F. Perin, E. Spessot, A. Famà, A. Bucciarelli, E. Callone, C. Mota, A. Motta and D. Maniglio, *ACS Biomater. Sci. Eng.*, 2023, **9**, 1320–1331.
23 J. M. Rios De La Rosa, A. Spadea, R. Donno, E. Lallana, Y. Lu, S. Puri, P. Caswell, M. J. Lawrence, M. Ashford and N. Tirelli, *Sci. Rep.*, 2020, **10**, 14505.
24 D. Nečas and P. Klapetek, *Open Phys.*, 2012, **10**, 181–188.
25 B. Lu, X. Lv and Y. Le, *Polymers*, 2019, **11**, 304.
26 H. M. Aldawsari, N. A. Alhakamy, R. Padder, M. Husain and S. Md, *Coatings*, 2020, **10**, 439.
27 N. G. Khlebtsov, *Anal. Chem.*, 2008, **80**, 6620–6625.
28 M. Chopin-Doroteo, E. A. Mandujano-Tinoco and E. Krötzsch, *Biochim. Biophys. Acta, Gen. Subj.*, 2021, **1865**, 129782.
29 A. Schwab, R. Levato, M. D'Este, S. Piluso, D. Eglin and J. Malda, *Chem. Rev.*, 2020, **120**, 11028–11055.
30 D. A. Rau, M. J. Bortner and C. B. Williams, *Addit. Manuf.*, 2023, **75**, 103745.
31 C. Minas, D. Carnelli, E. Tervoort and A. R. Studart, *Adv. Mater.*, 2016, **28**, 9993–9999.
32 S. S. L. Chan, R. M. Pennings, L. Edwards and G. V. Franks, *Addit. Manuf.*, 2020, **35**, 101335.
33 D. Kokkinis, M. Schaffner and A. R. Studart, *Nat. Commun.*, 2015, **6**, 8643.
34 A. M. Teixeira and P. Martins, *Front. Bioeng. Biotechnol.*, 2023, DOI: **10.3389/fbioe.2023.1161815**.
35 N. Shpaisman, L. Sheihet, J. Bushman, J. Winters and J. Kohn, *Biomacromolecules*, 2012, **13**, 2279–2286.
36 F. Perin, C. Mota, I. Mancini, A. Motta and D. Maniglio, *Polymer*, 2022, **252**, 124941.
37 S. Naghieh, M. D. Sarker, N. K. Sharma, Z. Barhoumi and X. Chen, *Appl. Sci.*, 2020, **10**, 292.
38 S. Naghieh and X. Chen, *J. Pharm. Anal.*, 2021, **11**, 564–579.
39 L. Ouyang, R. Yao, Y. Zhao and W. Sun, *Biofabrication*, 2016, **8**, 035020.
40 H. Chen, W. Yang, H. Chen, L. Liu, F. Gao, X. Yang, Q. Jiang, Q. Zhang and Y. Wang, *Colloids Surf., B*, 2009, **73**, 212–218.
41 C. Lee, J. S. Choi, I. Kim, K. T. Oh, E. S. Lee, E.-S. Park, K. C. Lee and Y. S. Youn, *Int. J. Nanomed.*, 2013, **8**, 2975–2983.
42 M. Trif, P. E. Florian, A. Roseanu, M. Moisei, O. Craciunescu, C. E. Astete and C. M. Sabliov, *J. Biomed. Mater. Res., Part A*, 2015, **103**, 3599–3611.
43 H. Tanaka, M. Matsumura and I. A. Veliky, *Biotechnol. Bioeng.*, 1984, **26**, 53–58.
44 A. Tirella, M. La Marca, L.-A. Brace, G. Mattei, J. W. Aylott and A. Ahluwalia, *J. Biomed. Nanotechnol.*, 2015, **11**, 1451–1460.